

Václav Kučera

The discontinuous Galerkin method for low-Mach flows

In: Jan Chleboun and Karel Segeth and Tomáš Vejchodský (eds.): Programs and Algorithms of Numerical Mathematics, Proceedings of Seminar. Prague, May 28-31, 2006. Institute of Mathematics AS CR, Prague, 2006. pp. 172–177.

Persistent URL: <http://dml.cz/dmlcz/702833>

**Terms of use:**

© Institute of Mathematics AS CR, 2006

Institute of Mathematics of the Czech Academy of Sciences provides access to digitized documents strictly for personal use. Each copy of any part of this document must contain these *Terms of use*.



This document has been digitized, optimized for electronic delivery and stamped with digital signature within the project *DML-CZ: The Czech Digital Mathematics Library*  
<http://dml.cz>

# THE DISCONTINUOUS GALERKIN METHOD FOR LOW-MACH FLOWS\*

Václav Kučera

## 1. Introduction

Our goal is to develop a numerical technique allowing the solution of compressible flow with a wide range of the Mach number. This technique is based on the *discontinuous Galerkin finite element method* (DGFEM), which employs piecewise polynomial approximations without any requirement on the continuity on interfaces between neighbouring elements. The DGFEM space semidiscretization is combined with a semi-implicit time discretization (Section 2.) and a special treatment of boundary conditions (Section 3.). In this way we obtain a numerical scheme requiring the solution of only one linear system on each time level. This scheme is successfully tested on flows with Mach numbers as low as  $10^{-4}$ . As for the transonic case it is necessary to avoid the Gibbs phenomenon manifested by spurious overshoots and undershoots in computed quantities near discontinuities and steep gradients. These phenomena do not occur in low Mach number regimes, however in the transonic case they cause instabilities in the semi-implicit solution. Here we present a possibility how to treat this problem (Section 4.). Section 5. presents computational results for small Mach numbers as well as transonic flow.

## 2. Discretization

We discretize the Euler equations in the conservative form:

$$\begin{aligned} \frac{\partial \mathbf{w}}{\partial t} + \sum_{s=1}^2 \frac{\partial \mathbf{f}_s(\mathbf{w})}{\partial x_s} &= 0 \quad \text{in } \Omega \times (0, T), \\ \mathbf{w} &= (\rho, \rho v_1, \rho v_2, e)^T \in \mathbb{R}^4, \\ \mathbf{f}_i(w) &= (\rho v_i, \rho v_1 v_i + \delta_{1i} p, \rho v_2 v_i + \delta_{2i} p, (e + p) v_i)^T. \end{aligned} \tag{1}$$

Let  $\mathcal{T}_h$  be a partition of  $\bar{\Omega}$  into a finite number of triangles with a numbering  $I$ . Let  $\Gamma_{ij} = \partial K_i \cap \partial K_j$  be a common edge of two triangles. The DGFEM uses the finite element space of discontinuous piecewise polynomial functions.

$$S_h = S^{p,-1}(\Omega, \mathcal{T}_h) = \{v; v|_K \in P_p(K) \ \forall K \in \mathcal{T}_h\}, \tag{2}$$

---

\*This work is a part of the research project No. MSM 0021620839 of the Ministry of Education of the Czech Republic. The research is partly supported by the Grant No. 6/2005/R of the Grant Agency of Charles University.

where  $P_p(K)$  is the space of all polynomials on  $K$  of degree  $\leq p$ . In the current implementation,  $P^0$ ,  $P^1$  and  $P^2$  approximations are used along with 5<sup>th</sup> order Gaussian quadrature rules on elements and edges.

We multiply (1) by a test function  $\boldsymbol{\varphi} \in [S_h]^4$  and integrate over  $K_i \in \mathcal{T}_h$ . With the aid of Green's theorem and summing over all  $i \in I$ , we obtain

$$\begin{aligned} \frac{d}{dt} \sum_{K_i \in \mathcal{T}_h} \int_{K_i} \mathbf{w} \cdot \boldsymbol{\varphi} dx &= \\ = \underbrace{\sum_{K_i \in \mathcal{T}_h} \int_{K_i} \sum_{s=1}^2 \mathbf{f}_s(\mathbf{w}) \cdot \frac{\partial \boldsymbol{\varphi}}{\partial x_s} dx}_{T_1} + \underbrace{\sum_{i \in I} \sum_{j \in S(i)} \int_{\Gamma_{ij}} \mathbf{H}(\mathbf{w}|_{\Gamma_{ij}}, \mathbf{w}|_{\Gamma_{ji}}, \mathbf{n}_{ij}) \cdot \boldsymbol{\varphi} dS}_{T_2}. \end{aligned} \quad (3)$$

In the term  $T_2$ , we have incorporated an approximation using a numerical flux  $\mathbf{H}$ , as known from the finite volume method. The approximate solution is defined as  $\mathbf{w}_h \in [S_h]^4$  such that (3) holds for all  $\boldsymbol{\varphi}_h \in [S_h]^4$ .

Scheme (3) represents a system of ordinary differential equations, which we must discretize with respect to time. Explicit time discretization is however undesirable due to a *CFL*-like condition, which limits the time step proportionally to the Mach number. A fully implicit scheme presents us with the task of solving a large nonlinear system on each time level. We therefore use the method presented in [4]. A forward Euler method is used and the nonlinear terms in the scheme are linearized. The resulting systems are solved using block-Jacobi preconditioned GMRES or the UMFPACK direct solver.

The term  $T_1$  in (3) is linearized using homogeneity of the Euler fluxes:

$$T_1 \approx \sum_{i \in I} \int_{K_i} \sum_{s=1}^2 \frac{D\mathbf{f}_s(\mathbf{w}_h^k)}{D\mathbf{w}} \mathbf{w}_h^{k+1} \cdot \frac{\partial \boldsymbol{\varphi}_h}{\partial x_s} dx. \quad (4)$$

As for the term  $T_2$ , the Vijayasundaram numerical flux is chosen, since it is suitable for linearization. This numerical flux has the form

$$\mathbf{H}_{VS}(\mathbf{w}_L, \mathbf{w}_R, \mathbf{n}) = \mathbb{P}^+ \left( \frac{\mathbf{w}_L + \mathbf{w}_R}{2}, \mathbf{n} \right) \mathbf{w}_L + \mathbb{P}^- \left( \frac{\mathbf{w}_L + \mathbf{w}_R}{2}, \mathbf{n} \right) \mathbf{w}_R. \quad (5)$$

### 3. Boundary conditions

The choice of appropriate boundary conditions is a delicate problem which plays a key role in the presented algorithm. Boundary conditions are incorporated into the DGFEM, as in the finite volume method, via the choice of  $H(\mathbf{w}_L, \mathbf{w}_R, \mathbf{n})$  or  $\mathbf{w}_R = \mathbf{w}|_{\Gamma_{ji}}$  for boundary edges. In the case of impermeable walls, we prescribe the *no-stick* condition  $\mathbf{v} \cdot \mathbf{n}$ . The situation is much more problematic on the inlet and outlet - standard boundary conditions reflect acoustic effects coming from the inside of  $\Omega$ . This behavior is nonphysical and the reflected interfering density and pressure

waves corrupt the solution in the low-Mach number case. To cure this disease new *characteristic based* boundary conditions are derived, which reflect the hyperbolic character of the Euler equations and are transparent to acoustic phenomena. These boundary conditions are a key ingredient in low-Mach calculations.

Using the rotational invariance and homogeneity we write the Euler equations in the nonconservative form

$$\frac{\partial \mathbf{q}}{\partial t} + \mathbb{A}_1(\mathbf{q}) \frac{\partial \mathbf{q}}{\partial \tilde{x}_1} = 0, \quad (6)$$

where  $\mathbf{q} = \mathbb{Q}(\mathbf{n})\mathbf{w}$  and  $\mathbb{Q}(\mathbf{n})$  is a standard  $4 \times 4$  rotational matrix (see [1]). We linearize this system around the state  $\mathbf{q}_i = \mathbb{Q}(\mathbf{n})\mathbf{w}_i$  and obtain a linear system. The goal is to choose the boundary state  $\mathbf{q}_j$  in such a way that this initial-boundary problem is well posed, i.e. has a unique solution. This linearized system has a solution which can be written explicitly using the method of characteristics. We shall take some state  $\mathbf{q}_j^0 = \mathbb{Q}(\mathbf{n})\mathbf{w}_j^0$ . The state  $\mathbf{w}_j^0$  is the state vector of the far-field flow. We calculate the eigenvectors  $\mathbf{r}_s, s = 1, \dots, 4$  of the matrix  $\mathbb{A}_1(\mathbf{q}_i)$ , arrange them as columns in the matrix  $\mathbb{T}$  and calculate  $\mathbb{T}^{-1}$  (explicit formulae can be found in [1]). We calculate

$$\boldsymbol{\beta} = \mathbb{T}^{-1}\mathbf{q}_i, \quad \boldsymbol{\alpha} = \mathbb{T}^{-1}\mathbf{q}_j^0. \quad (7)$$

Now we calculate the state  $\mathbf{q}_j$  according to the presented process:

$$\mathbf{q}_j := \sum_{s=1}^4 \gamma_s \mathbf{r}_s = \mathbb{T}\boldsymbol{\gamma}, \quad \gamma_s = \begin{cases} \alpha_s, & \lambda_s \geq 0, \\ \beta_s, & \lambda_s < 0 \end{cases} \quad (8)$$

and  $\lambda_s, s = 1, \dots, 4$  are eigenvalues of  $\mathbb{A}_1(\mathbf{q}_i)$ . Finally the sought boundary state is  $\mathbf{w}_j = \mathbb{Q}^{-1}(\mathbf{n})\mathbf{q}_j$ . Since we have respected the hyperbolic character of the Euler equations, these boundary conditions seem to give a natural choice for the boundary state  $\mathbf{w}_j$ .

#### 4. Shock capturing

Our approach is based on the discontinuity indicator  $g(i)$  proposed in [2] defined by

$$g(i) = \int_{\partial K_i} [\rho_h^k]^2 dS / (h_{K_i} |K_i|^{3/4}), \quad K_i \in \mathcal{T}_h. \quad (9)$$

We define a discrete shock indicator on the basis of (9):

$$G(i) = \begin{cases} 0, & g(i) < 1, \\ 1, & g(i) \geq 1. \end{cases}, \quad K_i \in \mathcal{T}_h.$$

To the left-hand side of (3) we add the form  $\beta(\mathbf{w}_h, \boldsymbol{\varphi}_h)$  defined by

$$\beta(\mathbf{w}, \boldsymbol{\varphi}) = C \sum_{i \in I} h_{K_i} G(i) \int_{K_i} \nabla \mathbf{w} \cdot \nabla \boldsymbol{\varphi} dx, \quad (10)$$

where  $C \approx 1$ . This artificial term represents a discrete Laplacian with zero Neumann boundary conditions on each element, thus forcing the solution to a piecewise constant function. The stabilization form  $\beta$  is treated implicitly (with  $G(i)$  computed from  $\mathbf{w}_h^k$ ).

This form limits the order of accuracy on each element lying on a discontinuity. However, it appears that on finely refined grids this is insufficient. Therefore, we propose to augment the left-hand side of (3) by adding the form  $J(\mathbf{w}_h, \boldsymbol{\varphi}_h)$  defined as

$$J(\mathbf{w}, \boldsymbol{\varphi}) = \varepsilon \sum_{i \in I} \sum_{j \in s(i)} \frac{1}{2} (G(i) + G(j)) \int_{\Gamma_{ij}} [\mathbf{w}] \cdot [\boldsymbol{\varphi}] dS, \quad (11)$$

where  $\varepsilon \approx 1$  and  $[u]|_{\Gamma_{ij}} = u_{ij} - u_{ji}$  is the jump on  $\Gamma_{ij}$  of a function  $u \in S_h$ . In this way we penalize inter-element jumps in the vicinity of the shock wave. This form can be treated implicitly, similarly as  $\beta(\mathbf{w}, \boldsymbol{\varphi})$ .

## 5. Numerical examples

In this section we present the solution of some test problems in order to demonstrate the accuracy and robustness of the proposed method. In all examples quadratic elements ( $r = 2$ ) were used for obtaining steady state solutions for " $t \rightarrow \infty$ ". The number of time steps necessary to obtain the steady state solution in the following test cases is approximately 100-200.

**1) Irrotational flow past a symmetric Joukowski airfoil** First we consider flow past a symmetric Joukowski profile with zero angle of attack. Using the complex function method from [3], we can obtain the exact solution of incompressible inviscid irrotational flow for this test case. We assume that the far field Mach number of compressible flow  $M_\infty = 0.0001$ . Figure 1 shows a detail near the profile of the

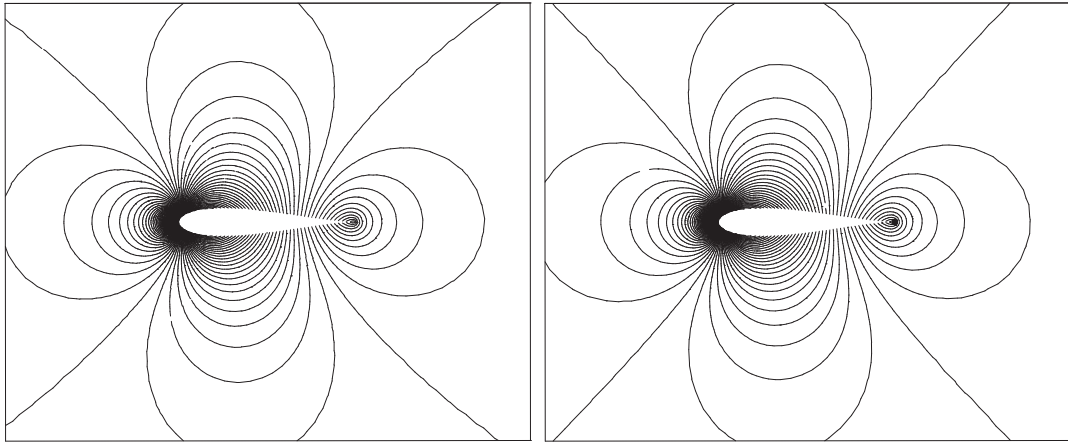


**Fig. 1:** Velocity isolines for the approximate solution of compressible flow (left) and for the exact solution of incompressible flow (right).

velocity isolines for the approximate solution of compressible flow and for the exact solution of incompressible flow, respectively. The mesh was formed by 4103 triangular elements.

**2) Irrotational flow past a nonsymmetric Joukowski airfoil** The second example deals with a similar problem to the preceding symmetric case. we present flow past a nonsymmetric Joukowski profile with zero angle of attack. Again, using the complex function method we can obtain the exact solution in the case of a non-symmetric Joukowski profile. The far field Mach number of is again  $M_\infty = 0.0001$ . Figure 2 shows a detail near the profile of the velocity isolines for the approximate solution of compressible flow and for the exact solution of incompressible flow, respectively. Figure 3 shows a comparison of the velocity distribution along the profile surface for the computed and exact solution. The mesh was formed by 5418 triangular elements.

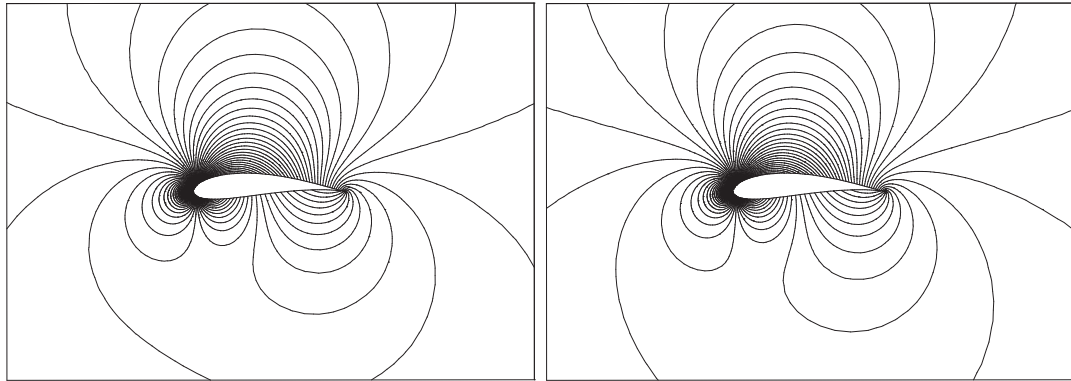


**Fig. 2:** Velocity isolines for the approximate solution of compressible flow (left) and for the exact solution of incompressible flow (right).

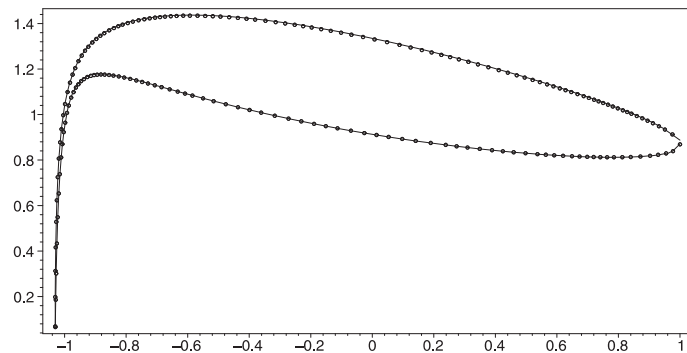


**Fig. 3:** Velocity distribution along the profile surface.  $\circ\circ\circ$  – exact solution of incompressible flow, —— approximate solution of compressible flow.

**3) Transonic flow** The performance of shock capturing terms from Section 4. is tested on the GAMM channel with a 10% circular bump and the inlet Mach number equal to 0.67. In this case a conspicuous shock wave is developed. Figure 4 shows Mach number isolines and entropy isolines computed by the presented scheme. One can see that this scheme yields the entropy production on the shock wave only, which is correct from the physical point of view. The stabilization parameters in were chosen  $\nu_1 = \nu_2 = 0.2$ . The mesh was formed by 7753 triangular elements.

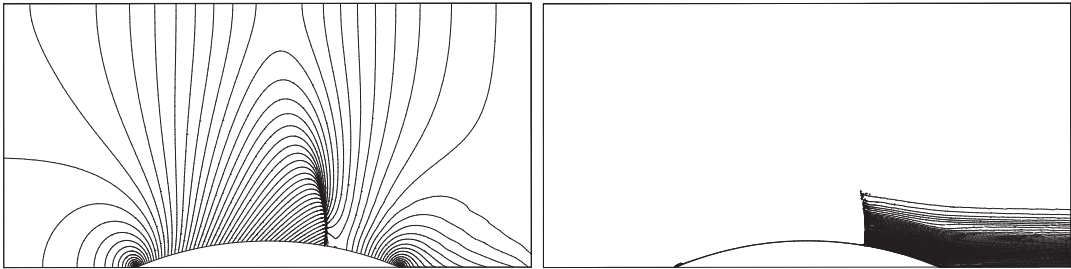


**Fig. 4:** GAMM channel transonic flow, Mach number (top) and entropy (bottom) isolines.

## References

- [1] Feistauer M., Felcman J., Straškraba I.: *Mathematical and Computational Methods for Compressible Flow*, Oxford University Press, Oxford, 2003.
- [2] V. Dolejší, M. Feistauer and C. Schwab. *On some aspects of the discontinuous Galerkin finite element method for conservation laws*. Math. Comput. Simul. **61**, 2003, 333–346.
- [3] M. Feistauer. *Mathematical Methods in Fluid Dynamics*. Longman Scientific & Technical, Harlow, 1993.
- [4] Dolejší V., Feistauer M.: *A Semi-Implicit Discontinuous Galerkin Finite Element Method for the Numerical Solution of Inviscid Compressible Flows*, The Preprint Series of the School of Mathematics MATH-KNM-2003/1, Charles University, Prague.